PNAS
www.pnas.org

Supplementary Information for

A multiscale biophysical model gives quantized metachronal waves in a lattice of beating cilia

Brato Chakrabarti, Sebastian Fürthauer, Michael J. Shelley

Sebastian Fürthauer, Michael J. Shelley
E-mail: sfuerthauer@flatironinstitute.org, mshelley@flatironinstitute.org

This PDF file includes:

Supporting Information Text

Parameters for active filament simulations

The dimensional internal parameters of the active filament model are estimated from previous experiments and simulations of a single cilium and *Chlamydomas* flagella. The typical magnitudes of these parameters are provided in Table S1.

Table S1. Table listing the numerical values of the dimensional parameters as reported in various experiments.

Parameter	Numerical Value	Description
a	$200\,n$m	Effective diameter of the axoneme (1)
L	$8-15\,\mu$m	Length of a typical cilium (2, 3)
B	$5\times10^{-23}-5\times10^{-22}$ N m^2	Range of possible bending rigidity (4–6)
K	2×10^{3} N m^{-2}	Inter-doublet elastic resistance measured for *Chlamydomonas* (7)
ν	$10^{-3}-10^{-2}$ Pa s	Range of viscosity in different media (7)
f_0	$2-5$ pN	Stall force for motor dynamics (7, 8)
f_c	$0.5-2.5$ pN	Characteristic unbinding force of the motors (1)
v_0	$5-7\,\mu$m/s	Motor walking speed at zero load (9)
τ_0	50 ms	Correlation time of motor activity (7, 10)
ρ	$10^{3}\,\mu$m^{-1}	Mean number density of motors (7, 10)

We can now estimate the dimensionless parameters of our internal mechanics model. For all the simulations used in the main text, we use the values listed in Table S2.

Table S2. Dimensionless parameters used for simulations in the main text.

Dimensionless number	Numerical value
$\mathrm{Sp}\equiv L\,(8\pi\nu/B\tau_0)^{1/4}$	2.5
$\mu_a\equiv af_0\rho L^2/B$	1.8×10^{3}
$\mu\equiv Ka^2L^2/B$	40
$\bar{f}\equiv f_0/f_c$	1.9
$\zeta\equiv a/v_0\tau_0$	0.3
$\eta\equiv\tau_0/(\tau_0+\epsilon_0)$	0.14

Properties of emergent waves

In the main text, we discuss how symplectic metachronal waves robustly emerge in finite beds of active filaments. Here we provide a few other quantitative characteristics of the emergent waves. First, we see from Fig. S1 that for both the active filaments and the rowers simulations the wavelength λ remains independent of the system size $\mathcal{N}$. For a given lattice spacing, the wavelength and all other properties are dependent only on the internal parameters of the system, the lattice spacing, and on the height h for the case of rowers.

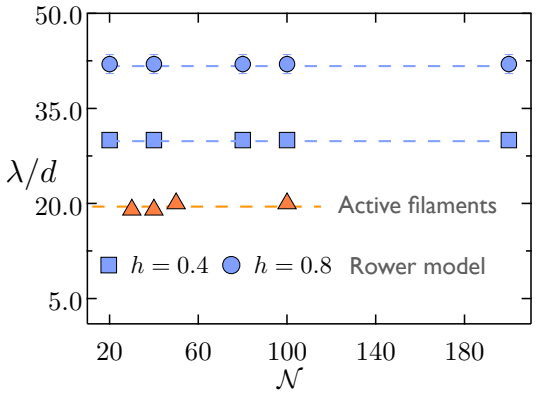

Fig. S1. Wavelength of the emerging metachronal wave from both the active filaments and the rowers model as a function of system size $\mathcal{N}$.

Figure. S2a shows the variation of the wavelength λ and the collective time period T of the emergent waves, normalized by the period of a single cilium T_0, as a function of the lattice spacing d. Consistent with previous simulations (11), we find that the wavelength decreases with increasing lattice spacing. However, there are minimal changes in the collective beating frequency compared to an independent single cilium. We attribute this primarily to the relatively sparse ciliary bed densities presently accessible to our simulations (12). We also point out that the specific nature of the variation of the wavelength as a function of lattice spacing depends on the internal model used for symmetry breaking of an individual cilium even though the qualitative behavior remains preserved.

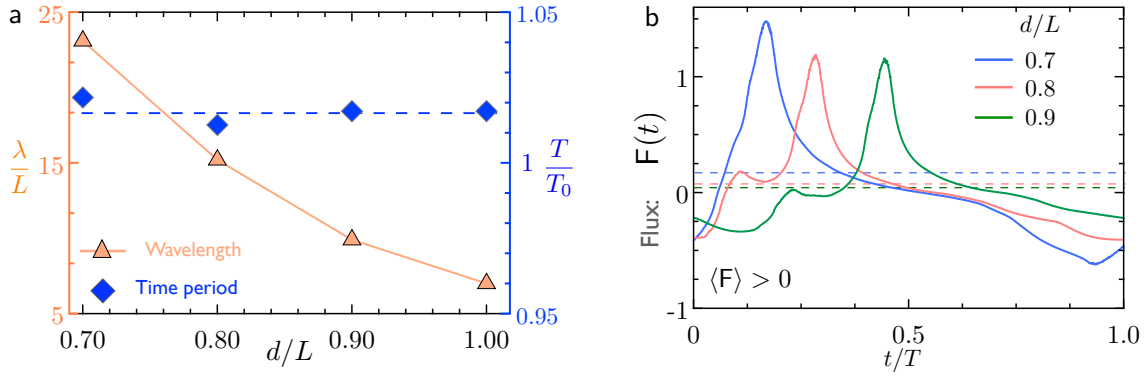

Fig. S2. a, Variation of the wavelength λ and the collective time period T as a function of the lattice spacing d. b, Instantaneous flux and mean pumping (dashed lines) over one time period for different lattice spacings.

Figure. S2b shows the instantaneous fluid flux $\mathsf{F}(t)$ over one period for different lattice spacings. The mean flux is indicated by the dashed lines. We find that there is a slight increase in mean pumping as the lattice spacing is reduced. Recent studies of collective behavior in a bed of active filament coupled solely through steric interactions have revealed that the emergent dynamics is sensitive to the amplitude of oscillations of individual filaments relative to their lattice spacing (13). Figure. S3 shows the amplitude computed from tip displacement of a filament in a metachronal wave does not vary as a function of the lattice spacing d/L. In contrast with (13), the ciliary beds considered in our simulations are much sparser. Thus, we are always in the regime that is dominated by hydrodynamic interactions. Steric interactions play an important role in preventing sharp phase-gradients. However, in the steady state, the waves are sustained purely through hydrodynamic interactions.

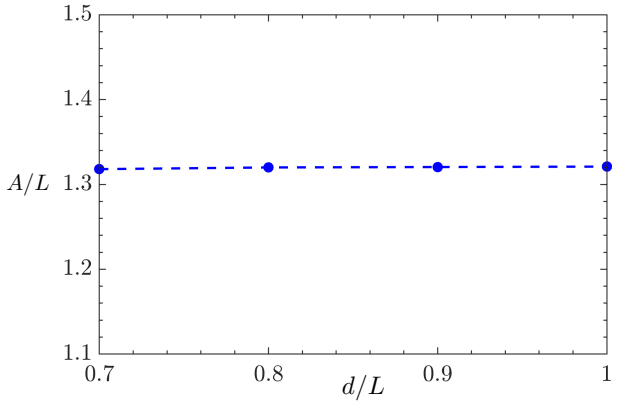

Fig. S3. Variation of the amplitude of oscillation A/L as a function of the spacing between the filaments.

Estimation of parameters for the rowers model

The dimensional form of the governing equation for the rowers model is given by:

$$\dot{x}_i = \frac{1}{6\pi\mu a}\left[F_0\sigma(1+\alpha\sigma) - \tilde{k}_e x_i\right] + u_i^d, \qquad [1]$$

where a is the radius of the bead, μ is the fluid viscosity, α is the asymmetry parameter, $\tilde{k}_e$ is the spring stiffness, and u_i^d is the disturbance flow field due to the presence of other particles and the wall. We non-dimensionalized length scales by the length of the tracks ℓ, time by a characteristic time-scale τ, and the disturbance flow field by $F_0/(8\pi\mu\ell)$. The dimensionless governing equation is then obtained as:

$$\dot{x}_i = F^*\left[\sigma(1+\alpha\sigma) - \frac{\tilde{k}_e\ell}{F_0}x\right] + F^*\frac{3a}{4\ell}u_i^d, \qquad [2]$$

where,

$$F^* = \frac{F_0 \tau}{6\pi\mu a \ell}. \quad [3]$$

In all our simulations we set $F^* = 1$. We can now try to relate all the parameters in the rowers model to the biophysical model of an individual cilium. The force scale F_0 can be mapped to the stall force of an individual dynein motor in the axoneme, thus $F_0 \sim 2$pN. The characteristic time scale τ is related to the inverse of beating frequency (f^{-1}) of a single cilium which is roughly $f \sim 10$Hz and the length of a cilium sets $\ell \sim 10\mu$m. Finally, we know that the bending rigidity of a cilium is $B \sim 10^{-22}$Nm^2. This allows us to estimate a spring stiffness $\tilde{k}_e \sim B/\ell^3$. Now setting $F^* = 1$ and using $\mu = \mu_{\text{water}}$ we find, $a \sim 1\mu$m which is the size of the bead used in our model. The dimensionless spring-constant is estimated as $k_e = \tilde{k}_e \ell / F_0 \sim 0.5$. The asymmetry parameter α was varied to investigate the role of left-right asymmetry in emergent dynamics.

Phase model and pair interactions

In the main text, we use a phase coupling model to elucidate a variety of emergent dynamics. Here we provide a brief outline of the derivation of the phase equations, starting from pair interactions. For a pair of filaments (or rowers) the evolution of their phase ψ can be written as

$$\dot{\psi}_1 = \omega + \varepsilon f(\psi_1, \psi_2), \quad [4]$$

$$\dot{\psi}_2 = \omega + \varepsilon f(\psi_2, \psi_1), \quad [5]$$

where ω is the natural frequency of oscillation and $f(\psi_1, \psi_2)$ is a coupling function that encodes the role of hydrodynamic interactions. We focus on the limit of weak coupling with $|\varepsilon| \ll 1$. In this limit, there is a separation of time scales as hydrodynamic interactions modify the phase dynamics over a slow time scale $\sim \varepsilon^{-1}$ while the phase grows linearly over a fast time scale $\sim \omega^{-1}$. The use of averaging with a two-time-scale expansion (14, 15) of the dynamics reveals that the coupling function should be of the form $f(\psi_1, \psi_2) = f(\psi_1 - \psi_2)$.

$$\dot{\psi}_1 = \omega + \varepsilon f(\psi_1 - \psi_2), \quad [6]$$

$$\dot{\psi}_2 = \omega + \varepsilon f(\psi_2 - \psi_1). \quad [7]$$

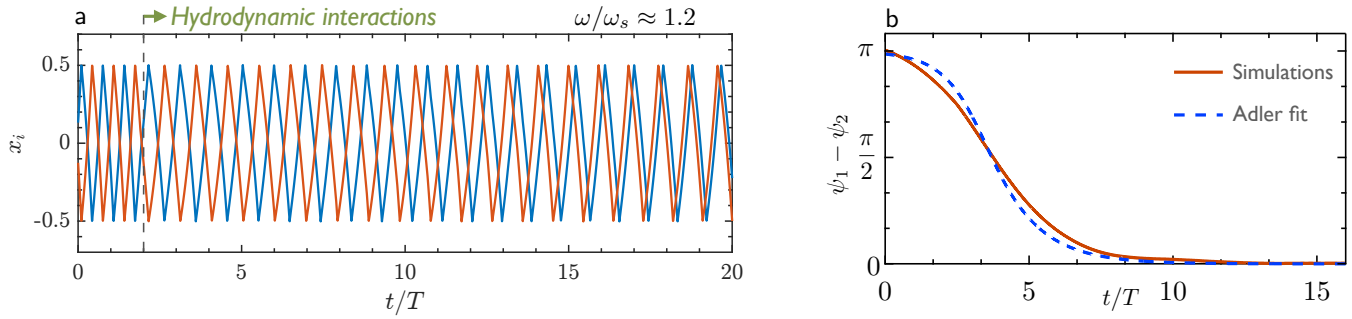

Fig. S4. a, We plot the position x_i of two rowers as a function of time. Initial conditions are chosen such that the rowers oscillate antiphase. As they start interacting hydrodynamically, their phase and frequency are altered. Finally the rowers are synchronized in-phase and they remain phase locked thereafter. The synchronous frequency ω_s is smaller than the individual frequency of isolated oscillators. b, We show the evolution of the phase difference between the rowers as a function of time. The blue line indicates the approximation to the simulations by the Adler equation.

Our previous work on the synchronization of active filaments (10) has demonstrated how the evolution of phase difference between two filaments is described by a Kuramoto-like coupling (16). Here we illustrate the same behavior for the minimal model of hydrodynamically coupled rowers. Figure. S4a shows the position x_i of two rowers that are initially oscillating almost anti-phase. Once they start interacting hydrodynamically, both their frequency of oscillation and their phases are altered and eventually, they are synchronized in-phase.

Figure. S4b shows the evolution of the phase difference between the rowers as a function of time. A simple choice of $f(\psi_1 - \psi_2) = \sin(\psi_1 - \psi_2)$ provides a decent fit to this phase evolution. This suggests that the phase difference $\delta = \psi_1 - \psi_2$ is reasonably approximated by the well-known Adler equation (15)

$$\dot{\delta} = \varepsilon \sin \delta. \quad [8]$$

For in-phase synchronization, we have $\varepsilon < 0$, which serves as the sole fitting parameter for the simulations. When the curvature of the harmonic potential $k_e > 0$, the rowers synchronize anti-phase (17).

As pointed out in (10, 18), for hydrodynamic interactions, the coupling constant ε can be related to the internal mechanics of active filaments. Following (18), we can estimate a scaling relation of the form:

$$\varepsilon \sim \frac{f_0^2 L}{B\mu d}. \quad [9]$$

The coupling strength is proportional to the active force scale set by the stall force f_0 of the motors and is inversely proportional to the viscosity of the medium. It is easier for floppier filaments with smaller bending rigidity B to synchronize faster. Finally, the scaling of $\varepsilon \sim 1/d$ stems from the fact that hydrodynamic interactions in free-space decays as $1/d$ (10). Due to the presence of screening from the walls we expect a faster decay of the coupling strength with distance.

Basin of attraction for traveling waves in rowers

In the main text, we have illustrated that a periodic lattice of rowers contain multiple attracting states. We quantified the basin of attraction of different states by computing the probability of formation of metachronal waves $\mathcal{P}_{\mathrm{MW}}$ as a function of two geometrical parameters: the lattice spacing d and the height h. In this section we show that while $\mathcal{P}_{\mathrm{MW}}$ is sensitive to the choices of internal parameters driving the rowers, the MW states still constitute a small part of the parameter space.

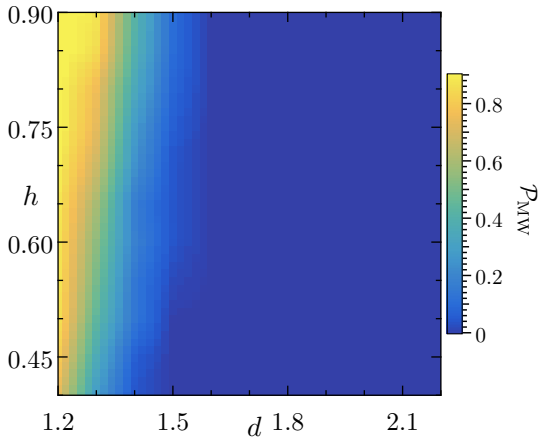

Fig. S5. Metachronal waves constitute a small portion of the entire parameter space as evident through our calculation of $\mathcal{P}_{\mathrm{MW}}$.

Models for asymmetric beating and collective dynamics

In order to have non-reciprocal, asymmetric beating patterns that mimic cilia we have introduced asymmetries in the detachment rate of dynein. We discussed this phenomenological law in great detail in the main text. For clarity we rewrite the detachment rate from the methods section as

$$\epsilon_{\pm} = \epsilon_0 n_{\pm} P_{\pm} \exp\left[\frac{|F_{\pm}|}{f_c}\right], \qquad [10]$$

where $n_{\pm}$ are the fractions of bound motors, $F_{\pm}$ are the forces exerted by individual dynein, f_c is a critical detachment force, and $P_{\pm}$ are the phenomenological coefficients ensuring asymmetry. We have made a specific choice for $P_{\pm}$ for all the results in the main text.

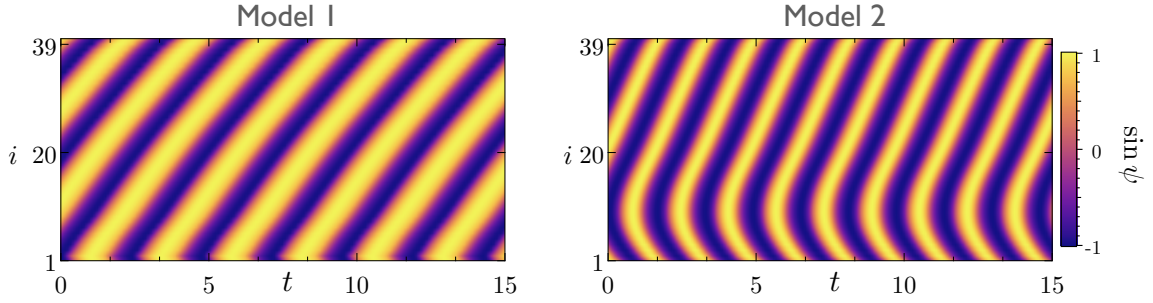

Fig. S6. Kymographs of phases for two different models of asymmetric beating. We have used 40 filaments in a finite lattice with $d/L = 0.8$.

In this section, we highlight that the results presented in the main text are independent of the choice of $P_{\pm}$. To illustrate this, we introduce two more choices of the phenomenological coefficients:

$$\text{Model 1:}\quad P_+ = \exp\left(\tilde{a}\dot{\Delta}\sin\phi_s/v_0\right) \text{ and } P_- = \exp\left(\tilde{b}\dot{\Delta}\cos\phi_s/v_0\right), \qquad [11]$$

$$\text{Model 2:}\quad P_+ = 1.3 \text{ and } P_- = 1, \qquad [12]$$

where $\tilde{a} = 0.8 f_0/f_c$ and $\tilde{b} = -0.6 f_0/f_c$. Figure. S6 shows the kymographs of emerging traveling waves on lattices with open boundaries for these two models. Figure. S7 shows the dynamics for Model 1 on a periodic lattice. In particular, we demonstrate

with our method of *cut-out-and-stitch-in* that the emergent state is again quantized by the charge $\mathcal{Q}$. In this case, we have designed a state with $\mathcal{Q} \approx 1$.

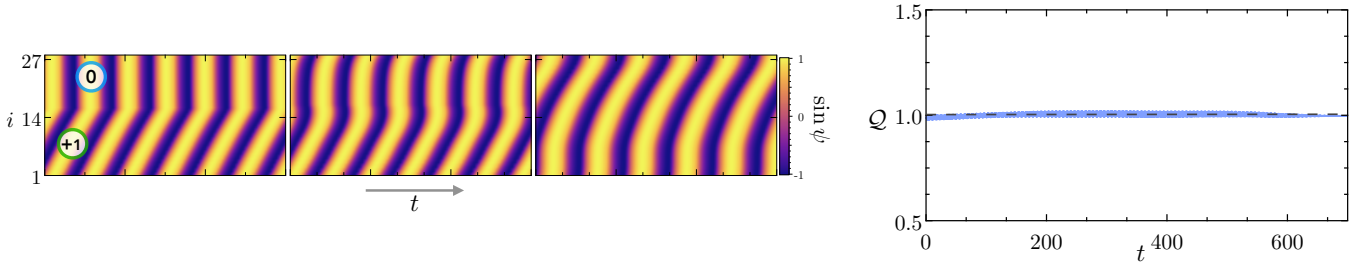

Fig. S7. Evolution of the kymograph of phase (left) for 28 active filaments following Model 1 on a periodic lattice with $d/L = 0.8$. We have stitched a solution with $\mathcal{Q} \approx 1$ with synchronous filaments. The charges carried by the two regions are marked on the initial kymograph. On the right we see the evolution of the charge $\mathcal{Q}$, which is approximately conserved.

Role of bending wave propagation direction in collective dynamics

In all of the simulations presented in the paper, the direction of wave propagation for an individual filament is from base-to-tip. For a single filament, there is a critical motor activity μ_a^c at which it starts to oscillate spontaneously due to the onset of a Hopf bifurcation. At the onset of this instability, the waves propagate from tip-to-base (retrograde) (1). As the activity is increased beyond μ_a^c, the direction of wave propagation switches to base-to-tip (anterograde). A comprehensive discussion on wave-propagation for an individual filament is done in our previous works (10, 19, 20). Here we focus on the role of wave-propagation on the emergent dynamics.

For anterograde wave propagation a pair of filaments synchronize in-phase. However with retrograde propagation, the scenario is reversed and a pair of filaments now synchronize anti-phase (AP). This fundamentally alters the collective dynamics in an array of such filaments. We now find that locally the filaments want to anti-align with its nearest neighbor. This prevents formation of long-wavelength metachronal waves. In the context of the phase-dynamics model, an AP synchronization translates to having a coupling constant $\varepsilon > 0$ for the evolution equation of the phase difference δ that reads $\dot{\delta} = \varepsilon \sin \delta$. The continuum analog of the phase-dynamics model requires smooth variation of the phase along the lattice. As a result, our continuum PDE is not applicable in the context of locally anti-phase oscillations. This in turn also points to the fact that the charge $\mathcal{Q}$ is not conserved in such a system. Figure S8 shows a snapshot of filament final conformations and the associated kymograph for this case.

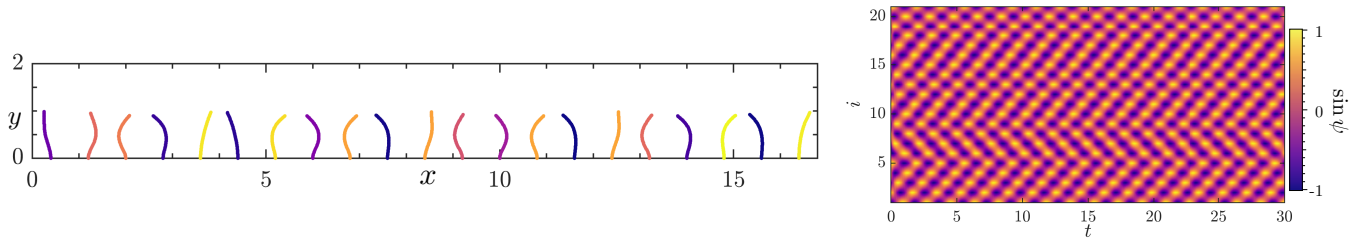

Fig. S8. Instantaneous filament conformations (left) and the associated kymograph (right) is shown for an array of active filaments with tip-to-base wave propagation. MWs are absent in this case and the filaments oscillate in anti-phase with its nearest neighbor. Parameter values: $\mathrm{Sp} = 6, \mu_a = 3\times10^3, \zeta = 0.3, \mu = 70, \bar{f} = 2, \eta = 0.14, P_\pm = 1$, and $d/L = 0.8$.

As discussed earlier, in the rowers model setting $k_e > 0$ gives rise to anti-phase oscillations between a pair of particles and this prevent formation of MWs. Consistent with the biophysical model, in a lattice of such rowers the particles oscillate anti-phase with its nearest neighbor. This is illustrated in the kymograph of Fig. S9. We initiated the simulation with phase-locked rowers which corresponds to a fixed point of the system with periodic boundary conditions. However as seen in Fig. S9 this fixed point is unstable.

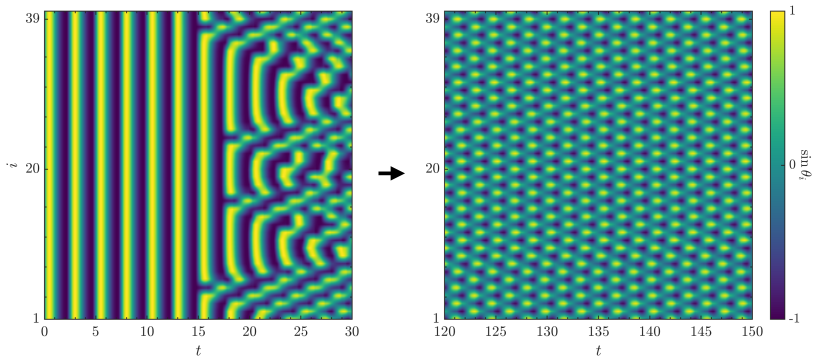

Fig. S9. Phase evolution in an array of 40 rowers with $k_e > 0$. The rowers spontaneously evolve to a state of locally anti-phase oscillations that is reminiscent of collective dynamics of active filaments with tip-to-base wave propagation. Parameter values: $k_e = 0.6, \alpha = 0.3, d = 1.3$.

Quantized states in the follower force model

Our prediction on quantized states was based on a general phase dynamics model and were supported by detailed simulations of a relevant biophysical model. Since the phase dynamics model is independent of the microscopic physics, it is worthwhile to investigate its predictions in other models of active filaments. We partially addressed this question in the previous section, where we showed that the charge is approximately preserved independently of the response of molecular motors. Now we consider the 'follower-force' (21–23) model of spontaneously beating active filaments to explore the robustness of our predictions. In this simplified model, the filament centerline is modeled as an inextensible Euler elastica. However, the internal machinery of the axoneme that generates active moments is neglected. The action of molecular motors is coarse-grained as the line density of compressive forces that act parallel to the local tangent to the centerline. Using slender-body theory (SBT),

$$\partial_t \mathbf{x}(s,t) = \mathcal{M} \cdot \left(-B\mathbf{x}_{ssss} + (T\mathbf{x}_s)_s - \sigma \mathbf{x}_s\right), \qquad [13]$$

where $\mathcal{M}$ is the mobility defined by the SBT. The force per unit length has contributions from bending with bending rigidity B, tension T that enforces inextensibility, and σ that accounts for the force generated by the molecular motors. Beyond a critical value of σ this system supports a Hopf bifurcation, leading to spontaneous symmetric oscillations of the filament. Just as with the results presented in the main text, finite beds of these filaments lead to formation of waves. Due to their symmetric oscillations, the waves split from the middle of the domain and propagate on either side, as seen in the kymographs in Fig. S10.

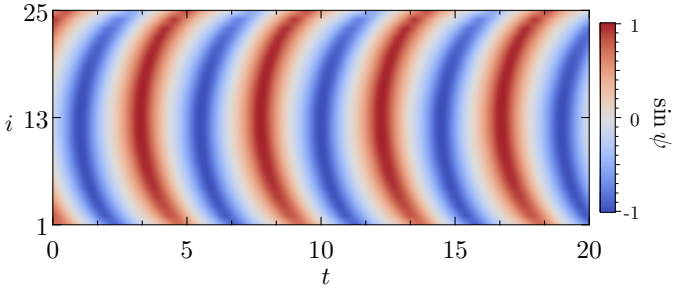

Fig. S10. Wave splitting on a finite bed of active filaments modeled with the follower-force model.

We now follow our *cut-out-and-stitch-in* method to design an initial condition with charge $\mathcal{Q} \approx 1$ in a periodic lattice of these filaments. An evolution of this, shown in Fig. S11, illustrates the diffusive dynamics of phase and the approximate conservation of charge $\mathcal{Q}$.

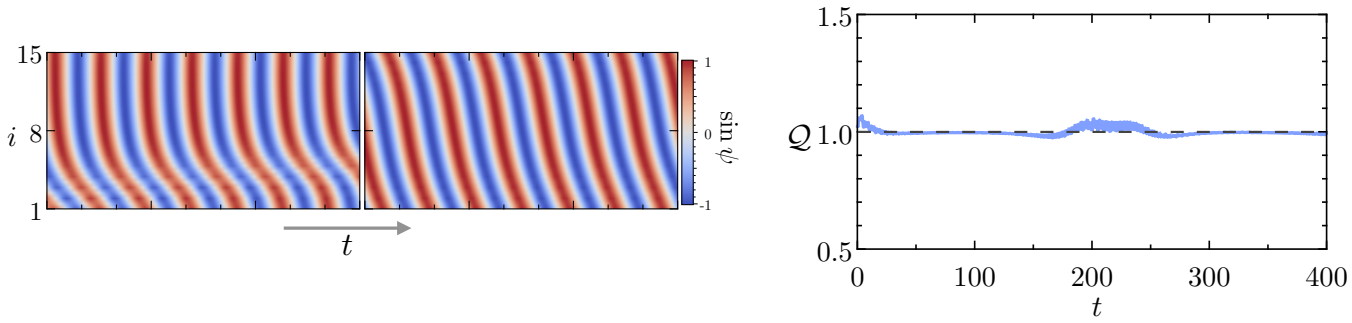

Fig. S11. Evolution of the kymograph of phases for 15 filaments from the follower-force model, in a periodic lattice. The initial conditions are designed to have charge $\mathcal{Q} \approx 1$ which is approximately conserved during the evolution.

Recently Sangani and Gopinath (24) performed a linear stability analysis for a carpet of cilia actuated by the follower-force model. Their analysis in periodic lattice with non-local SBT accounts for hydrodynamic interactions among all the filaments. Their results suggest that depending on the magnitude of the follower force, the emergent dynamics at the linear order is either in-phase or anti-phase oscillations. Our results are in partial agreement with these findings. In a periodic lattice, when the filaments are perturbed by Fourier modes, they always synchronize in-phase. However, in our simulations with follower-force model, we have not observed anti-phase dynamics. This is most likely the effect of nonlinear interactions between various unstable modes that are absent in the linear analysis (24).

Role of short-range interactions in charge conservation

In the main text we have speculated that charge conservation in our biophysical model is a result of short-range steric and hydrodynamic interactions that prevent appearance of sharp phase gradients. In the rowers model the phase evolution is characterized by defects and thus the charge $\mathcal{Q}$ is not conserved. This is further illustrated in Fig. S12. We design an initial state of rowers with $\mathcal{Q} \approx 0$. However, hydrodynamic interactions lead to the formation of metachronal wave with $\mathcal{Q} \approx 3$. Some of the phase defects during the transient is marked in red circles and the charge is not conserved.

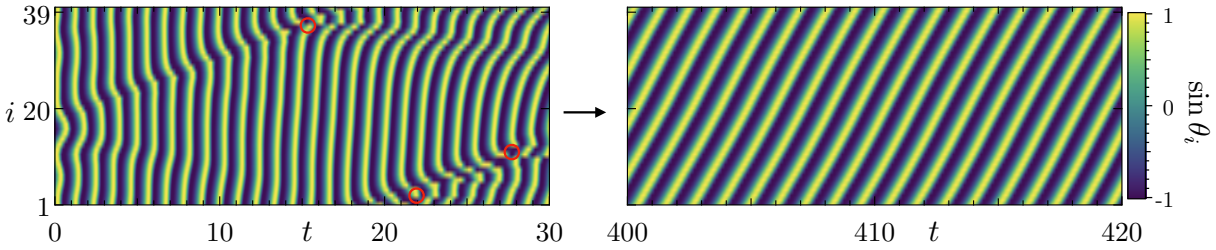

Fig. S12. Evolution of the kymograph of phases for $N = 40$ rowers on a periodic lattice. The red circles indicate some of the phase defects during the initial stages of evolution. The initial state has $\mathcal{Q} \approx 0$ and the final state has $\mathcal{Q} \approx 3$. This illustrates that the charge is not conserved.

Role of noise in emergent dynamics

Cilia is a stiff filament with its persistence length ℓ_p being larger than its length L. However, intrinsic to the microscopic processes involving the attachment and detachment of molecular motors that drive oscillations in a single filament is biochemical noise. In this section we first consider the role of the biochemical noise in charge conservation. In presence of noise, the evolution equation for the bound motor population reads:

$$\partial_t n_\pm(s,t) = \pi_\pm(s,t) - \epsilon_\pm(s,t) + \eta_\pm, \qquad [14]$$

where $\pi_\pm$ and $\epsilon_\pm$ are the attachment and detachment rates respectively and the last term indicates the thermal fluctuation. We have $\langle \eta_\pm \rangle = 0$, and $\langle \eta_\pm(s,t)\eta_\pm(s',t') \rangle = 2\tilde{\Lambda}\delta(t-t')\delta(s-s')$, where $\tilde{\Lambda}$ plays the role of an effective temperature. The fluctuations primarily lead to perturbations in the phase kymograph. Figure S13 shows the evolution of the charge $\mathcal{Q}$ as a function of time in a homogeneous bed designed with $\mathcal{Q} = 1$ for two different values of the effective temperature.

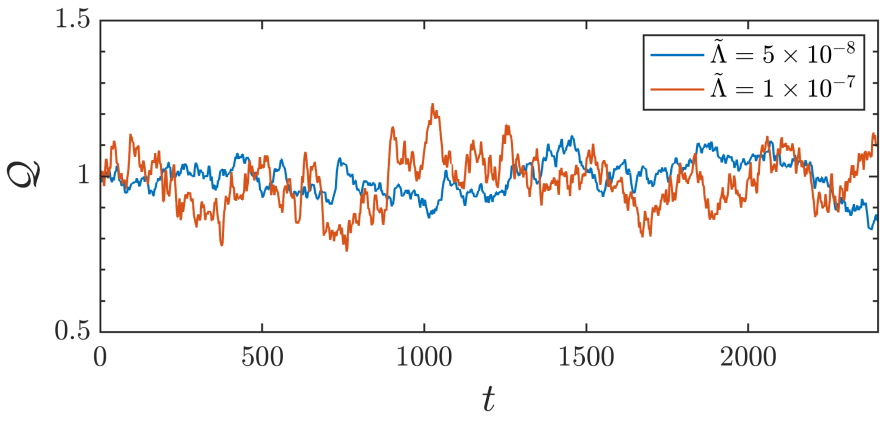

Fig. S13. Evolution of the charge $\mathcal{Q}$ as a function of time for two different effective temperatures.

These simulations highlight an important point that the charge $\mathcal{Q}$ is approximately conserved even in the presence of biochemical noise. One way to break charge conservation will be to introduce phase-defects. While biochemical noise can potentially provide a pathway for this, the steric interactions in our present model prevents such topological defects.

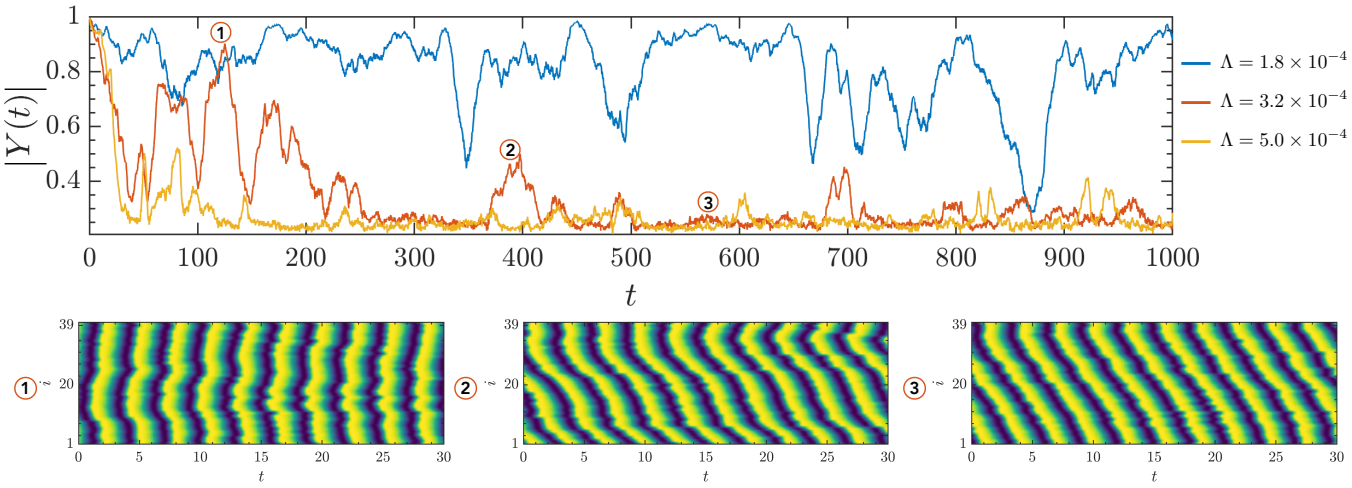

Fig. S14. Phase evolution in an array of 40 rowers for different effective temperatures Λ. We show three kymographs from different instances for $\Lambda = 3.2 \times 10^{-4}$. Parameter values: $k_e = -0.6, \alpha = 0.3, d = 1.5, h = 0.4$.

Our discussion in the previous section already highlights that the absence of short-range interaction in the rowers model prevents charge conservation. This also means that biochemical noise may provide a generic pathway in this minimal model for transitions between different attractors. To consider this, we solve the stochastic version of the rowers equation that is given by:

$$\dot{x}_i = \sigma(1 + \alpha\sigma) - kx_i + \frac{3a}{4\ell} u_i^d + \eta_i. \qquad [15]$$

Like before, $\langle \eta_i \rangle = 0$ and $\langle \eta(t)\eta(t') \rangle = 2\Lambda\delta(t - t')$, and Λ serves as the effective temperature. Here we have performed a set of simulations by varying the effective temperature Λ at a fixed separation distance d, and height h for the rowers. In order to quantify the synchronization we introduced the Kuramoto order parameter $Y(t) = \sum_i \exp(\mathrm{i}\theta_i)$. When all the oscillators are phase-locked we have $|Y| = 1$. Figure S14 shows the evolution of the order parameter for different Λ. The simulations were initiated with a phase-locked state of $|Y| = 1$. For weak noise the oscillators remain trapped in the attractor it starts with. But with increasing noise it can intermittently jump to other attractors. We show three characteristic kymographs from the long time-series for a given Λ. These kymographs highlight the hopping between phase-locked state (1) and multiple MW states (2 and 3). For even larger noise, the kymographs are punctured by phase-defects.

Preliminary results on various 2D lattice arrangements

Our paper highlights that an understanding of the charge $\mathcal{Q}$ equips us with designing patchy lattices that always develop waves. Our main focus has been in understanding dynamics of 1D lattices. However, our preliminary results show that many of the ideas that we have explored in great detail for 1D lattices translate for other lattice arrangements in 2D. At the heart of this is the three-dimensional non-local hydrodynamics that we have considered in all of our simulations. In this section we highlight a set of preliminary results that show the universality of the dynamics in other lattice arrangements.

Role of heterogeneity. We first consider a homogeneous 2D bed of filaments arranged on a square lattice. We have used a plane-wave perturbation as the initial condition for the filament arrangement. This perturbation sets the initial charge $\mathcal{Q} \approx 0$. Figure S15 shows that the charge is conserved and the whole bed of filaments get phase-locked over time.

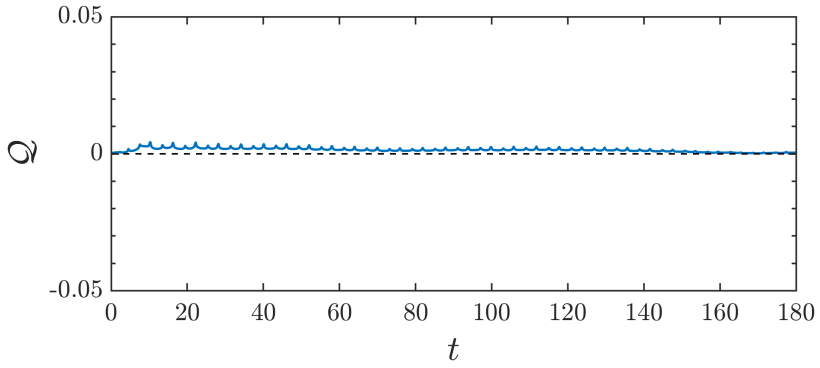

Fig. S15. Evolution of the charge $\mathcal{Q}$ in a 2D lattice of $16 \times 16 = 256$ filaments with periodic boundary conditions. The simulations were initiated with a plane wave-perturbation that sets $\mathcal{Q} \approx 0$. Over time, the charge is conserved and the system is driven to a phase-locked state.

In order to illustrate the role of patched arrangements in 2D, we consider a patch from the previous lattice with identical initial conditions. A snapshot of the filament configuration is shown in Fig. S16 along with a kymograph that shows the phase evolution with time along different rows of the lattice. The white lines in the kymograph indicate the beginning of different rows. This setup is the 2D analog of the 1D arrangement considered in Fig. 5(b) of our main draft.

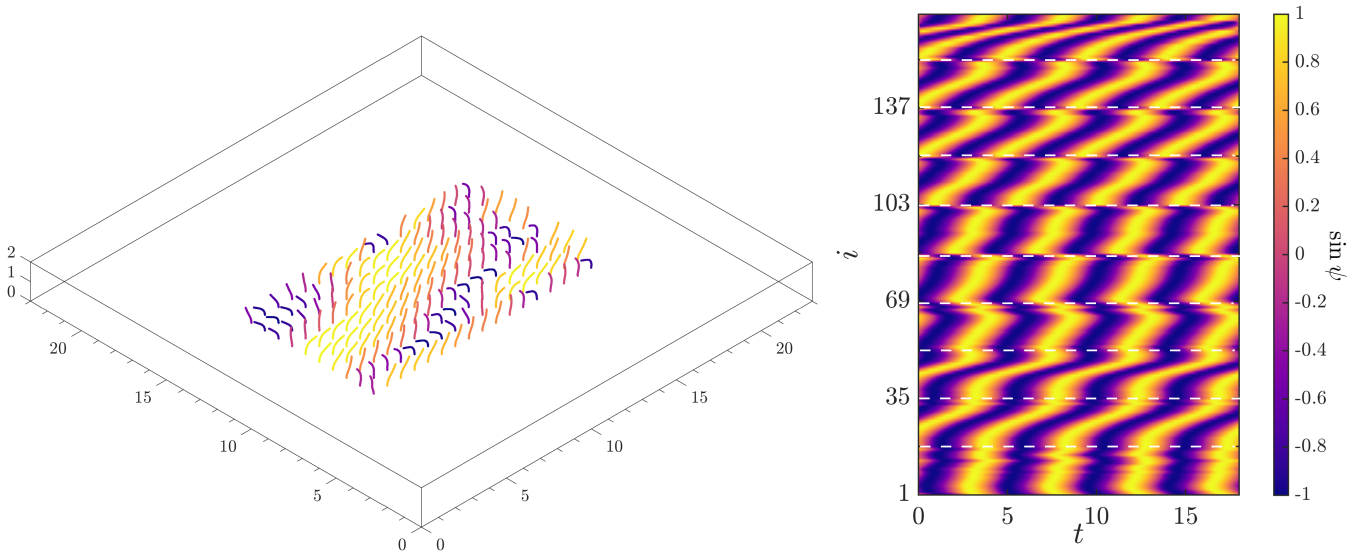

Fig. S16. Instantaneous snapshot of filaments developing MW in a 2D patch of $17 \times 10 = 170$ filaments and the associated kymograph. The white lines in the kymograph indicate different rows in the lattice. The patch was taken out of the synchronously beating 2D homogeneous bed described in the previous example.

Charge conservation. In order to understand how the idea of charge conservation can be generalized we consider two distinct ciliary arrangements as described below.

- **Orthoplectic ciliary rows:** Orthoplectic rows are a variation of the 1D arrangement considered in our paper. In an orthoplectic row of cilia the filaments are arranged in equal spacing, orthogonal to the beating plane. Hydrodynamics in such an array is fundamentally different from the planar arrays considered by us. Recent simulations suggest (25) that filaments in orthoplectic rows can spontaneously form disordered states that are suitable for pumping.

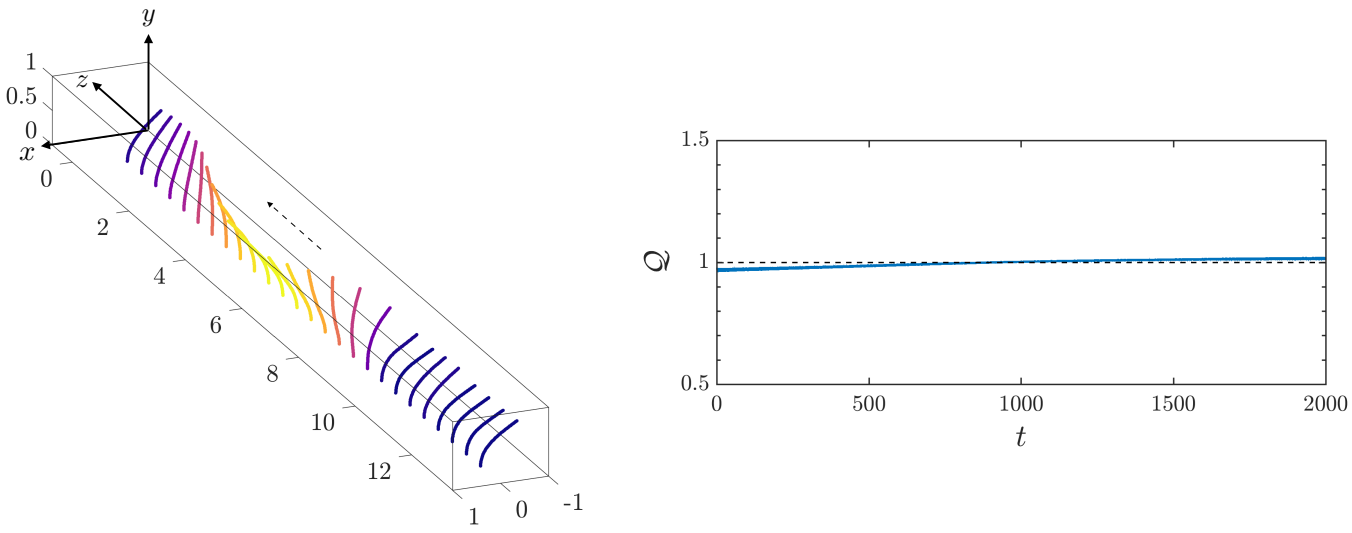

Fig. S17. Evolution of the charge $\mathcal{Q}$ in an orthoplectic row of active filaments. A snapshot of the propagating wave is shown on the left.

In order to test the charge conservation, we designed a state with $\mathcal{Q} = 1$ and imposed periodic boundary condition along the the z direction. Figure S17 shows a snapshot of propagating MWs and the associated evolution of $\mathcal{Q}$ that indicates conservation of charge.

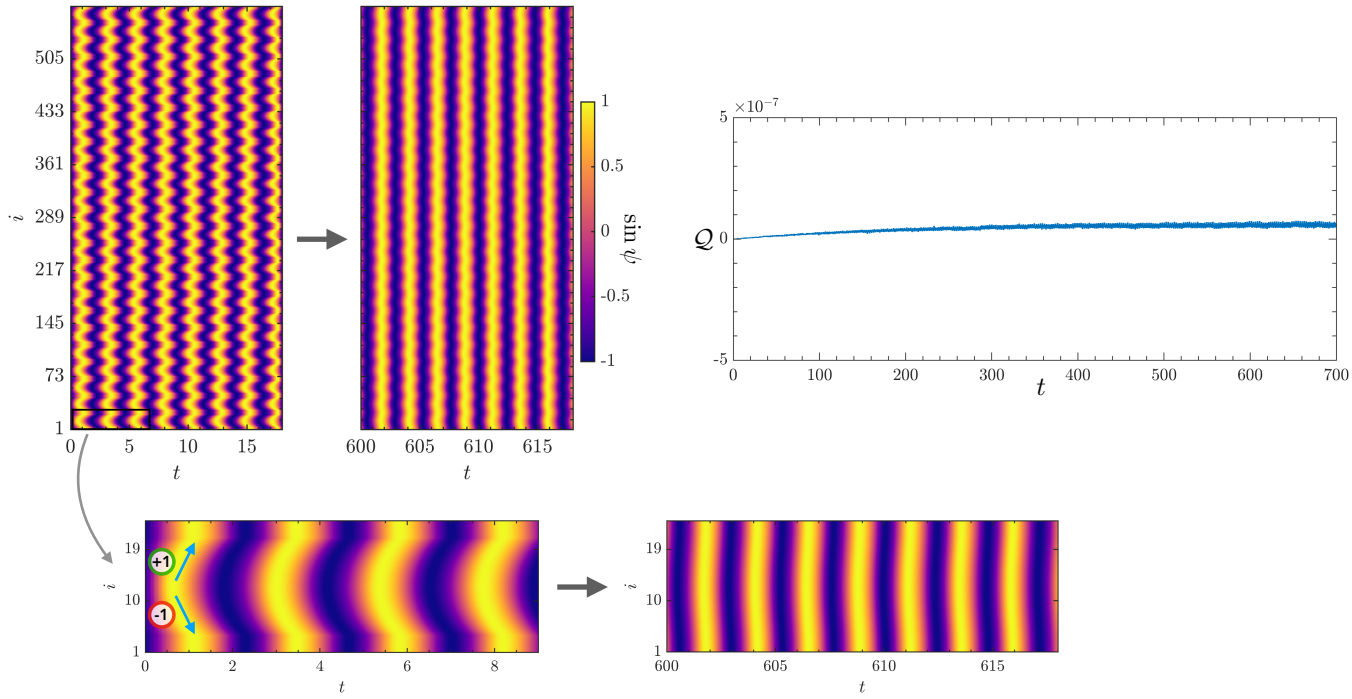

Fig. S18. We design initial state of $\mathcal{Q} = 0$ by our method of 'cut-out-and-stitch-in'. The kymograph shows the evolution of the phases in a lattice of $24 \times 24. = 576$ filaments. A zoomed version of the kymograph for a row shows the charge carried by different portions and the arrows indicate the direction of wave propagation. Evolution of the charge $\mathcal{Q}$ shows it is conserved as the system gets phase-locked. We emphasize that these are not quasi 2D simulations as the lattice was generated by coping the cut out strip along both the reciprocal vectors of the square lattice.

- **A 2D 'cut-out-and-stitch-in':** We now consider an implementation of our method of 'cut-out-and-stitch-in' in homogeneous 2D square lattice of cilia. We first consider a 1D row of charge zero constructed by stitching $\mathcal{Q} = \pm 1$ along with a stripe of $\mathcal{Q} = 0$ filaments. We then create a 2D plane wave-state by copying this ciliary array along both the reciprocal lattice vectors. In the Fig. S18 we highlight the evolution of the charge $\mathcal{Q}$. This illustrates conservation of charge and the kymographs indicate that the system is driven towards a phase-locked state.

Summary of key results

We have used a hierarchy of models to understand the role of various interactions that shape the dynamics of ciliary arrays. In table. S3 we provide a brief summary of the key features and main results from the various models.

Table S3. Summary of various models and their respective predictions.

Model	Interactions	Results
Biophysical Model	Hydrodynamic and steric	1. MWs on finite lattices 2. Multiple states on periodic lattice 3. States characterized by invariant integer charge
Rowers	Hydrodynamic	1. MWs on finite lattices 2. Multiple states on periodic lattice 3. No charge conservation
Phase dynamics model	Nearest neighbor coupling	1. Multiple states on periodic lattice 2. Continuum PDE predicts quantized states and charge conservation

List of supplementary videos

- **Movie S1:** Symmetric beating of a single cilium. Corresponds to Fig. 1**c** of the main text.
- **Movie S2:** Asymmetric beating of a single cilium. Corresponds to Fig. 1**c** of the main text.
- **Movie S3:** Phase evolution of 40 symmetric rowers showing wave splitting in a finite lattice. Corresponds to Fig. 2**a** of the main text.
- **Movie S4:** Wave splitting in an array of 24 active filaments with symmetric beating patterns in a finite lattice. Corresponds to Fig. 2**c** of the main text.
- **Movie S5:** Metachronal wave in a finite lattice of 40 asymmetric rowers. Corresponds to Fig. 2**b** of the main text.
- **Movie S6:** Symplectic metachronal waves in an array of 24 filaments with asymmetric beating patterns in a finite lattice. Corresponds to Fig. 2**e** of the main text.
- **Movie S7:** Filament centerlines from Movie S6 is now color coded by the distribution of motors. We also show dynein activity on a single filament from the lattice and illustrate the time delay between sliding displacement and motor activity.
- **Movie S8:** Metachronal waves in a periodic array of 40 rowers. Corresponds to Figure 3**b** of the main text.
- **Movie S9:** Metachronal waves in a homogeneous bed of 62 active filaments with charge $\mathcal{Q} \approx 3$. We also show the evolution of the bound motor population n_+ at the tip of the filaments $s = 1$. Corresponds to Figure 5**a** of main text.
- **Movie S10:** Metachronal waves in a periodic array of 70 filaments with spatial heterogeneity. Corresponds to Fig. 5**c** of the main text.
- **Movie S11:** Metachronal wave in patches of 99 filaments on a periodic lattice. We also show the evolution of the bound motor population n_+ at the tip of the filaments $s = 1$. Corresponds to Figure 5**e** of the main text.
- **Movie S12:** We show the role of steric interactions and hydrodynamic interactions mediated by filament contact or near-contact in a periodic lattice of 38 filaments. The contacts of the filaments are particularly evident near the edges and in the middle of the lattice. For this simulation $d/L = 0.7$.

References

1. IH Riedel-Kruse, A Hilfinger, J Howard, F Jülicher, How molecular motors shape the flagellar beat. *HFSP journal* **1**, 192–208 (2007).
2. M Sleigh, The form of beat in cilia of stentor and opalina. *J. Exp. Biol.* **37**, 1–10 (1960).
3. H Machemer, Ciliary activity and the origin of metachrony in paramecium: effects of increased viscosity. *J. Exp. Biol.* **57**, 239–259 (1972).
4. M Hines, J Blum, Bend propagation in flagella. i. derivation of equations of motion and their simulation. *Biophys. J.* **23**, 41–57 (1978).
5. S Gueron, N Liron, Ciliary motion modeling, and dynamic multicilia interactions. *Biophys. journal* **63**, 1045–1058 (1992).
6. G Xu, et al., Flexural rigidity and shear stiffness of flagella estimated from induced bends and counterbends. *Biophys. journal* **110**, 2759–2768 (2016).
7. D Oriola, H Gadêlha, J Casademunt, Nonlinear amplitude dynamics in flagellar beating. *Royal Soc. open science* **4**, 160698 (2017).
8. E Hirakawa, H Higuchi, YY Toyoshima, Processive movement of single 22s dynein molecules occurs only at low atp concentrations. *Proc. Natl. Acad. Sci.* **97**, 2533–2537 (2000).
9. J Howard, , et al., *Mechanics of motor proteins and the cytoskeleton.* (Sinauer associates Sunderland, MA) Vol. 743, (2001).
10. B Chakrabarti, D Saintillan, Hydrodynamic synchronization of spontaneously beating filaments. *Phys. review letters* **123**, 208101 (2019).
11. J Elgeti, G Gompper, Emergence of metachronal waves in cilia arrays. *Proc. Natl. Acad. Sci.* **110**, 4470–4475 (2013).
12. N Pellicciotta, et al., Entrainment of mammalian motile cilia in the brain with hydrodynamic forces. *Proc. Natl. Acad. Sci.* **117**, 8315–8325 (2020).
13. R Chelakkot, MF Hagan, A Gopinath, Synchronized oscillations, traveling waves, and jammed clusters induced by steric interactions in active filament arrays. *Soft Matter* **17**, 1091–1104 (2021).

14. CM Bender, SA Orszag, *Advanced mathematical methods for scientists and engineers I: Asymptotic methods and perturbation theory*. (Springer Science & Business Media), (2013).
15. A Pikovsky, J Kurths, M Rosenblum, J Kurths, *Synchronization: a universal concept in nonlinear sciences*. (Cambridge university press) No. 12, (2003).
16. Y Kuramoto, *Chemical oscillations, waves, and turbulence*. (Courier Corporation), (2003).
17. C Wollin, H Stark, Metachronal waves in a chain of rowers with hydrodynamic interactions. *The Eur. Phys. J. E* **34**, 1–10 (2011).
18. KY Wan, RE Goldstein, Coordinated beating of algal flagella is mediated by basal coupling. *Proc. Natl. Acad. Sci.* **113**, E2784–E2793 (2016).
19. B Chakrabarti, D Saintillan, Spontaneous oscillations, beating patterns, and hydrodynamics of active microfilaments. *Phys. Rev. Fluids* **4**, 043102 (2019).
20. B Chakrabarti, *Problems on Viscous Dynamics of Passive and Active Microfilaments*. (University of California, San Diego), (2019).
21. P Bayly, S Dutcher, Steady dynein forces induce flutter instability and propagating waves in mathematical models of flagella. *J. The Royal Soc. Interface* **13**, 20160523 (2016).
22. G De Canio, E Lauga, RE Goldstein, Spontaneous oscillations of elastic filaments induced by molecular motors. *J. The Royal Soc. Interface* **14**, 20170491 (2017).
23. F Ling, H Guo, E Kanso, Instability-driven oscillations of elastic microfilaments. *J. The Royal Soc. Interface* **15**, 20180594 (2018).
24. AS Sangani, A Gopinath, Elastohydrodynamical instabilities of active filaments, arrays, and carpets analyzed using slender-body theory. *Phys. Rev. Fluids* **5**, 083101 (2020).
25. J Han, CS Peskin, Spontaneous oscillation and fluid–structure interaction of cilia. *Proc. Natl. Acad. Sci.* **115**, 4417–4422 (2018).